Available online at www.sciencedirect.com

ScienceDirect

Procedia IUTAM 22 (2017) 184 – 191

Procedia IUTAM

www.elsevier.com/locate/procedia

IUTAM Symposium on Nonlinear and Delayed Dynamics of Mechatronic Systems

Response robustness and safety against jump to contact in AFMs controlled via different techniques

Valeria Settimi[a], Giuseppe Rega[a,*]

[a]*Department of Structural and Geotechnical Engineering, Sapienza University of Rome, Via A. Gramsci 53, Rome 00197, Italy*

Abstract

The role of a global dynamics analysis to assess a system robustness and actual safety in operating conditions is investigated by studying the effect of different local and global control techniques on the nonlinear behavior of a noncontact AFM via dynamical integrity concepts and tools.

Peer-review under responsibility of organizing committee of the IUTAM Symposium on Nonlinear and Delayed Dynamics of Mechatronic Systems

Keywords: Dynamical Integrity; Noncontact AFM; Nonlinear Dynamics; Feedback Control; Global Control.

1. Introduction

Analyzing the nonlinear dynamical behavior of a mechanical system usually entails the investigation of the stability of its response under variation of some (characterizing and/or controllable) parameter. Bifurcation diagrams and eventually behavior charts in parameters space allow to verify the system robustness to possible changes of the operational parameter setup, and often reveal a wide variety of nonlinear phenomena, such as bifurcations and in-well instability regions which can lead to possible unstable, aperiodic or chaotic oscillations. However, besides these analyses, possible changes in the system initial conditions due to imperfections have to be taken into account, since it is nowadays ascertained that the safe operation of a nonlinear system depends not only on the local stability of its solutions but also on the global dynamics associated with the uncorrupted basin surrounding each solution [1]. This is certainly true for the currently very popular micro/nano mechanical systems, for which slight changes of the initial position and/or velocity at the nanoscale level can produce dramatic modifications of the overall dynamics. Among them, Atomic Force Microscopes (AFMs) working in noncontact mode can undergo the unwanted "jump to contact" phenomenon, or escape (in dynamical systems terms), due to the atomic attraction between the cantilever tip and the sample to be scanned which can become stronger than the beam restoring elastic force making the equilibrium configuration unstable and producing contacts between tip and sample responsible for errors in the topography process. From a global dynamics perspective, it is thus of interest to clearly detect in the state plane the basins of attraction

* Corresponding author. Tel.: +39-06-49919195 ; fax: +39-06-49919192.
E-mail address: giuseppe.rega@uniroma1.it

Peer-review under responsibility of organizing committee of the IUTAM Symposium on Nonlinear and Delayed Dynamics of Mechatronic Systems
doi:10.1016/j.piutam.2017.08.027

(i.e. the union of all possible initial conditions) of the periodic (acceptable) solutions and that of the (undesirable) unbounded response compromising the device operation. Furthermore, the relevant erosion process due to variations of some system parameter (usually the excitation amplitude) can be followed and quantified by means of the construction of the so-called erosion profiles. As a practical consequence of such analyses, which belong to the field of dynamical integrity, the sensitivity of a system to variations of both operational parameters and initial conditions can be discussed, and some hints useful to define thresholds able to ensure acceptable safety targets can be achieved.

Within this general framework, dynamical integrity is proposed as a comprehensive approach for comparatively evaluating the effects of different control techniques to be possibly employed for securing the AFM response robustness and safety against jump to contact. Attention is focused, in particular, on two conceptually different techniques: (i) an external feedback control frequently applied to AFM devices and tailored to improving their local dynamics[2], and (ii) a control which exploits the global properties of the AFM response in view of improving its overall dynamics[3].

2. AFM model and control techniques

As reference system, a model of noncontact AFM is considered (Fig. 1(a)), whose reduced order equation of motion reads[4]:

$$\ddot{x} + \alpha_1 x + \alpha_3 x^3 = -\frac{\Gamma_1}{(1+x)^2} - \rho_1 \dot{x} + x\mu_1 U\omega^2 sin(\omega t) \tag{1}$$

where $x(t)$ is the microcantilever tip transverse displacement; dot denotes the time derivative; α_1 and α_3 are linear and cubic stiffness coefficients; ρ_1 is the linear damping coefficient; Γ_1 is the attractive atomic interaction coefficient; ω and U are frequency and amplitude of the horizontal parametric scan excitation. In the state plane, the relevant unperturbed system shows the presence of a single potential well with a stable equilibrium, delimited by the homoclinic orbit of the single hilltop saddle (Fig. 1(b)), which separates the bounded solutions from the unbounded ones leading to the well-known jump to contact phenomenon responsible for the failure of the scan operation.

To avoid the occurrence of such unstable responses, which would compromise the correct characterization of the sample, several feedback control techniques are commonly applied to the AFM[2]. Thus, a simple external feedback control is added to the continuum formulation of the AFM model, with the objective to maintain the microcantilever vibration close to an operationally suitable reference response obtained for the uncontrolled system with the same set of parameters values. The corresponding single-mode reduced equations are[5]:

$$\ddot{x} + \alpha_1 x + \alpha_3 x^3 = -\frac{\Gamma_1}{(1+x+z-z_s)^2} - \rho_1 \dot{x} + x\mu_1 U\omega^2 sin(\omega t) \qquad \dot{z} = k_g(x_{ref} - x) \tag{2}$$

where $z(t)$ is the control variable representing the distance of the fixed side of the microcantilever from the horizontal reference axis; k_g is the external feedback control parameter; z_s is the displacement of the sample surface from the selected reference position, and $x_{ref}(t)$ the reference periodic response of the uncontrolled system, solution of eq. (1) (see Fig. 1(c)).

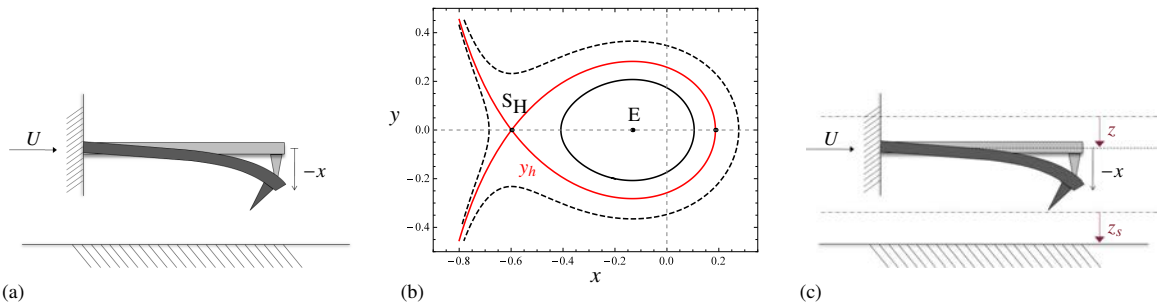

Fig. 1. AFM microcantilever (a), unperturbed phase space (b) for $\alpha_1 = 1, \alpha_3 = 0.1, \Gamma_1 = 0.1$. In (b), homoclinic orbit y_h (solid red), periodic orbit (solid black), unbounded orbit (dashed black), equilibrium point (E), hilltop saddle point (S_H) are reported. AFM microcantilever with external feedback control (c).

The global dynamics of this feedback controlled model has been already investigated[6] by systematically constructing 2D cross-sections of the five-dimensional basins of attraction, and by obtaining the relevant erosion profiles for increasing excitation amplitude. The erosion process has been quantified by means of two different integrity measures[7], the Global Integrity Measure (GIM) and the Integrity Factor (IF), respectively accounting for and getting rid of the basins fractal parts. The overall outcomes in terms of dynamical integrity highlight a meaningful worsening of the system practical stability in the excitation frequency-amplitude plane (Fig. 2(a)), especially around the natural resonance frequency $\omega = 0.8358$.

Thus, moving from a local to a global perspective, a different control method[3] based on exploiting the global properties of the dynamical system has to be implemented, in order to possibly preserve the system dynamical integrity by reducing the safe basin erosion which leads to the loss of safety. The method consists of optimally modifying the shape of the excitation to delay the occurrence of the global events (i.e., homo/heteroclinic bifurcations of some saddle) which trigger the erosion (i.e., the sudden fall in the erosion profiles), thus obtaining an overall control of the dynamics and an enlargement of the system safe region in parameters space. Following the method, controlling superharmonics of amplitudes U_j and phases Ψ_j are added to the harmonic excitation of the AFM model (1):

$$\ddot{x} + \alpha_1 x + \alpha_3 x^3 = -\frac{\Gamma_1}{(1+x)^2} - \rho_1 \dot{x} + x\mu_1 \omega^2 U_1 \sum_{j=1}^{n} \frac{U_j}{U_1} sin(j\omega t + \Psi_j) \tag{3}$$

where U_1 represents the harmonic forcing amplitude. The numerical procedure applied to detect the optimal superharmonic requires the numerical detection of the saddle(s) involved in the bifurcation responsible for the profiles fall down, and the implementation of a tailored routine able to compute the maximum distance between the relevant manifolds, among all those calculated for varying controlling amplitudes.

The effects of the global control on the AFM dynamics have been analyzed at the forcing frequency $\omega = 0.7$[8], which is around the left-shifted non linear resonance ensuing from the system softening response[9], by adding a single superharmonic 2ω to the harmonic excitation, consistent with the asymmetric feature of the system unperturbed phase-portrait in Fig. 1(b) (so-called one-side control). In this case, upon identifying the homoclinic bifurcation actually triggering the erosion – which involves a (secondary) saddle different from the hilltop one –, numerical implementation of the control technique with optimal amplitude $U_2/U_1 = -0.32$ has proven to be effective in reducing the basins fractalization and postponing the penetration of the tongues of the unbounded basin inside the potential well. This entails a shift of the global event and simultaneously a delay of the fall down of the erosion profile, thus increasing the system overall safety.

In the light of the obtained results, and in order to allow a comprehensive comparison of the effects of the proposed control techniques on the system global dynamics, additional analyses are developed, focusing on two different frequencies, $\omega = 0.7$ and $\omega = 0.9$, representative of the system behavior around primary resonance. Of course, com-

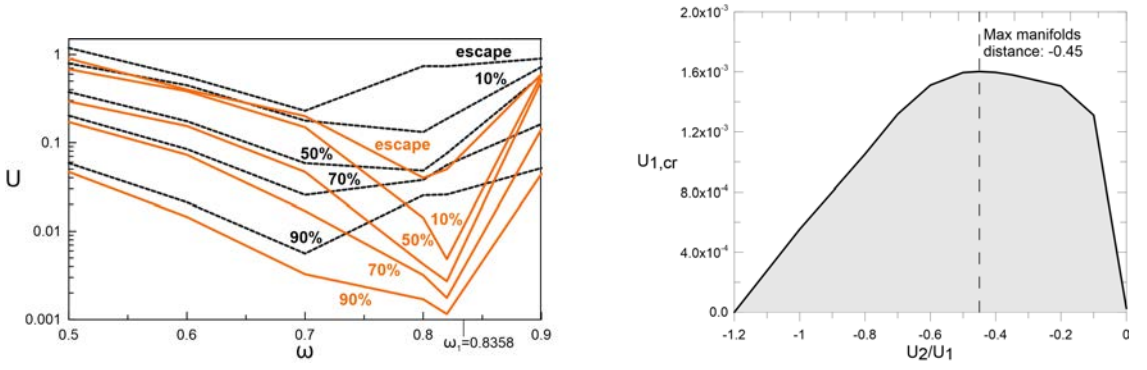

(a) (b)

Fig. 2. Residual iso-GIM curves of the system safe basin up to jump-to-contact (escape), for the reference system (black, dashed lines) and for the system with feedback control (orange, solid lines) (a). Threshold of the homoclinic bifurcation $W^u_I(S_1) \cap W^s_I(S_1)$ as a function of the superharmonic amplitude U_2/U_1, at $\omega = 0.9$ (b).

parison of the two control techniques could be made just at this resonance, where – based on Fig. 2(a) – the effects of the feedback control on the dynamical integrity are especially detrimental. However, the behavior of the system manifolds is therein particularly complicated and tangled, so that the application of the global control is numerically too onerous. Moreover, as it will be shown forward, the topological scenarios of the varying basins of attraction at $\omega = 0.7$ and $\omega = 0.9$ are interestingly different from each other already for the reference system, and entail different qualitative patterns of the integrity profiles. This makes the comparison with the two control techniques particularly worth.

It is also worth underlining that to apply the global control at $\omega = 0.9$, one odd superharmonic (3ω) is added to the harmonic forcing, different from what done at $\omega = 0.7$. This is related just to the behavior of the basins of attraction, which for high values of the forcing amplitude – where the profiles sharply fall down – are organized in the state plane so as to assume a configuration similar to two symmetric potential wells (see the third attractor-basin portrait in the Fig. 4(a) forward), which are optimally controlled by odd superharmonics (so-called two-side control)[7]. The homoclinic bifurcation of the left manifolds of the internal saddle separating the two basins is numerically controlled by applying the controlling amplitude $U_2/U_1 = -0.45$, which represents the optimal value, as shown in Fig. 2(b).

3. Response robustness of the system with different controls

It is of interest to discuss the effects of the aforementioned control techniques on the robustness of the periodic responses depicted by the system. To this aim, the evolution of the relevant basins of attraction is analyzed for increasing values of the harmonic forcing amplitude, and the results are reported in Figs. 3 and 4 for $\omega = 0.7$ and $\omega = 0.9$, respectively. It is worth to note that the reference and the globally controlled systems are 2-dimensional in the state plane, while the system with feedback control is 5-dimensional. As a consequence, the basins reported here for the latter are planar sections of the 5D basins, obtained by fixing 3 of the 5 initial conditions for the system variables, i.e. ($x = x_{ref}$,$y = y_{ref}$,$z = 0$), which appear to be the most reasonable set up from an operational point of view[5], and their realization has to be carried out by means of computationally burdensome ad hoc routines.

Analyzing the basins of the reference system, a qualitatively different behavior can be observed before and after the resonance frequency. For frequencies lower then the resonant one, in fact, the system shows the contemporary and competing presence of two 1-period resonant/nonresonant responses (red/blue basins of Fig. 3(a)), which ends up to a complete replacement of the latter by the former with further increasing values of the excitation[9]; instead, after the resonance, only one 1-period solution dominates the potential well, apart from splitting in two 1-period solutions for high values of the forcing amplitude, as shown in the two nearby continuous black branches of the bifurcation diagram in Fig. 5(a), and in the third and fourth portraits of Fig. 4(a).

Starting from these situations, the addition of the external feedback control into the model causes a generalized increasing of the erosion due to the enlargement of the basin of the unbounded solution (white basin in Figs. 3 and 4), which develops mainly to the detriment of the non-dominant responses. Due to the feedback control, in fact, the basin of the resonant solution at $\omega = 0.7$ disappears, as well as the basins of the high period solutions at $\omega = 0.9$. At this frequency, moreover, the feedback control is able to properly reproduce the 1-period solution only in a defined range of the harmonic forcing amplitude, after which the periodic responses depicted by the system cannot be considered acceptable anymore. To better clarify this aspect, the bifurcation diagrams as a function of the forcing amplitude are reported in Fig. 5, for the system with feedback control (orange lines) and for the reference one (black lines). The comparison shows the onset of a new transcritical bifurcation, which unstabilizes the 1-period solution at $U = 0.598$, and represents the limit of applicability of the feedback control. After that, in fact, the stable solutions of the controlled system (whose basins are indeed reported in different colors in the last two portraits of Fig. 4(b)) do not reproduce the reference solutions (i.e. $z \neq z_s = 0.01$, see Fig. 5(c)), highlighting the bad control operation.

Unlike the feedback control, the global one has the explicit objective to increase the overall robustness of the system, an issue which is successfully accomplished with also beneficial effects on the main solutions displayed by the system, whose basins of attraction are either made less fractal (Fig. 3(c)) or actually enlarged (Fig. 4(c)). Specifically, before the resonance the separation of the core-dominant nonresonant basin from the resonant one rolling on its border is shifted to higher values of the harmonic forcing amplitude, without modifying the topological behavior of the system. This aspect can be observed by comparing the safe basins of Fig. 3(a) with the corresponding basins of Fig. 3(c), which are identified by the black circle reported upon the basins and associated with the computation of

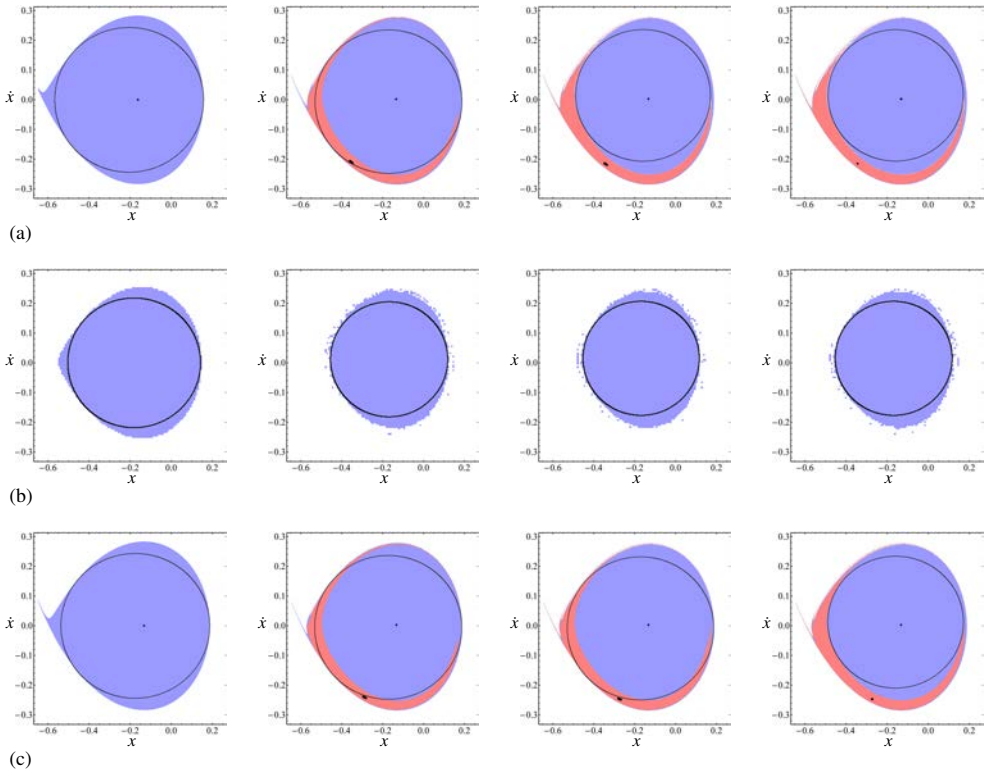

Fig. 3. Attractor-basin phase portraits at $\omega_u = 0.7$ and $U = 0$, $U = 0.006$, $U = 0.00697$, $U = 0.007$, for the reference system (a) and for the system with global control (c); cross-sections of the basins of attraction for the system with feedback control (b). The black circle represents the IF measure of the safe basin.

the Integrity Factor. At $U = 0.00697$, the safe basin of the reference system coincides with the sole nonresonant (blue) 1-period solution, while for the globally controlled system it still corresponds to the union of the resonant and nonresonant basins. After the resonance, on the other side, the robustness of the (blue) dominant basin is increased by delaying the arise of the competing 1-period solution (red basin in the last two portraits of Fig. 4(a)), so that the topology of the basins of the globally controlled system for some values of U results significantly different with respect to the reference case (see comparison between the third portraits of Fig. 4(a) and 4(c)).

Finally, it is worth noting that although the feedback control has some detrimental effect on the behavior of the system with respect to the response robustness, it is able, when properly working, to exactly reproduce the reference response, as shown in Fig. 6 where the two responses are overlapped. Conversely, in the global control, the addition of the superharmonic slightly modifies the amplitude and the shape of the system responses.

4. Safety against jump to contact of the system with different controls

For AFM models, avoiding the contact between the cantilever tip and the sample to be scanned (the so-called jump to contact phenomenon) is of great importance in order to guarantee the correct topography operation. In dynamical integrity terms, it corresponds to analyzing the robustness of the system safe basin with respect to the erosion due to the unbounded solution basin, corresponding to the set of initial conditions leading to the jump to contact. From the results presented in the previous section, it can be deduced that for the reference system and for the globally controlled one the safe basin is the union of the basins of attraction of the bounded solutions inside the potential well, while for the system with feedback control it is reduced to the sole response properly controlled, i.e. the basin of the dominant (nonresonant) 1-period solution.

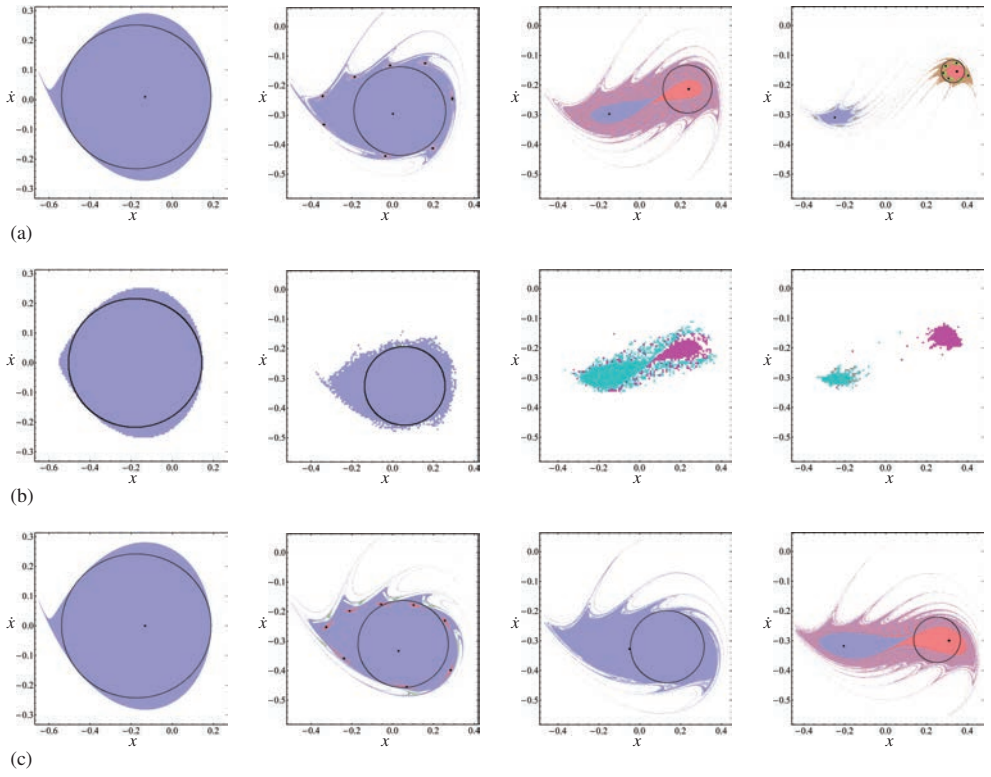

Fig. 4. Attractor-basin phase portraits at $\omega_u = 0.9$ and $U = 0$, $U = 0.5$, $U = 0.65$, $U = 0.75$, for the reference system (a) and for the system with global control (c); cross-sections of the basins of attraction for the system with feedback control (b). The black circle represents the IF measure of the safe basin.

To quantify the erosion of the safe basin, the GIM and IF integrity measures are applied, and the erosion profiles as a function of the harmonic forcing amplitude are built. The comparison among the results obtained for the three systems is reported in Figs. 7 and 8, before and after the resonance frequency, respectively. It is worth noting the different pattern of the decreasing profiles obtained already for the reference system at the two frequencies. The former (Fig. 7(a)) exhibit a sharp, though relatively limited, fall down, followed by a long and smooth decrease down

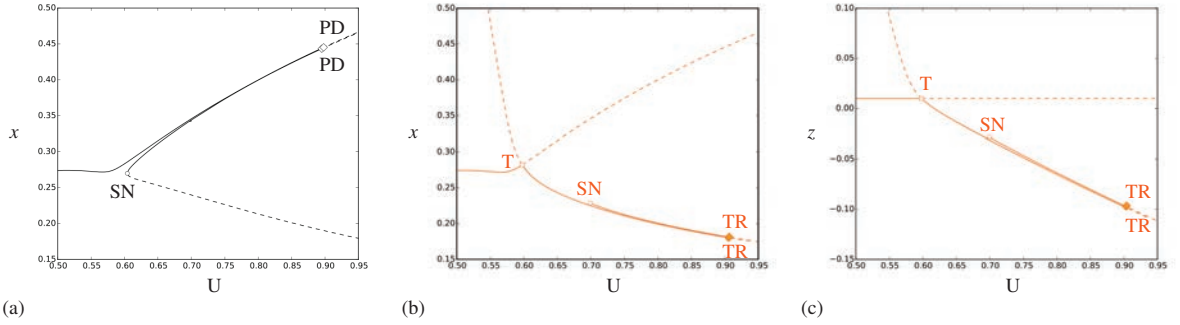

Fig. 5. Bifurcation diagram as a function of the forcing amplitude U, at $\omega = 0.9$, for the reference system (black lines/bifurcations) (a). Bifurcation diagram with respect to the displacement variable x (b) and to the control variable z (c), for the system with feedback control (orange lines/bifurcations). SN: saddle-node bifurcation; T: transcritical bifurcation; PD: period-doubling bifurcation; TR: torus bifurcation.

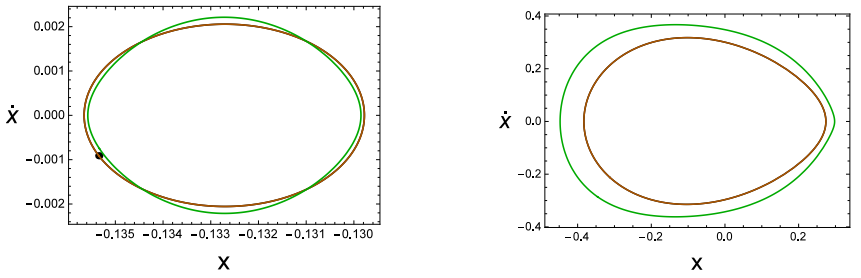

(a) (b)

Fig. 6. Periodic solutions in the state plane at $\omega = 0.7$ and $U = 0.006$ (a) and $\omega = 0.9$ and $U = 0.5$ (b), for the reference system (black solution), for the system with feedback control (orange solution) and for the system with global control (green solution).

to zero; the latter (Fig. 8(a)) show an inverted sequence of the two intervals, with a final sharp fall down which is definitely wider. In both cases, attention is focused on the sharp part of the profiles, which marks the loss of safety for the system, represented by the sudden reduction of the percentage of safe basin residual integrity.

When applying the global control, the profile fall down is shifted to higher values of the harmonic forcing amplitude, enlarging the range of U values in which the system safety is guaranteed, while leaving the qualitative trend of the profiles substantially unchanged, as can be observed by comparing the green and black profiles in both Fig. 7(b) and Fig. 8(b). From such comparison, furthermore, it appears that at $\omega = 0.9$ the global control is even more effective than at $\omega = 0.7$, likely due to being farther away from the left-shifted nonlinear resonance. In the case of the feedback control, conversely, the reduction of the safe basin to the sole 1-period dominant basin causes the lowering of the profiles in the whole range of forcing amplitude, however with some differences. At $\omega = 0.7$ (orange profiles of Fig. 7(b)), the erosion develops smoothly, without sudden falls as in the reference and the globally controlled cases; this feature is worthily kept, at this frequency, also at higher excitation amplitudes, as highlighted by the nearly constant intervals in-between the successive (orange) iso-GIM curves of Fig. 2(a). In this sense, despite its lower integrity level, the system with feedback control turns out to be more robust than the others with respect to possible safety changes. Looking at the behavior at $\omega = 0.9$, (orange profiles of Fig. 8(b)), on the contrary, the limit value $U = 0.598$, responsible for the birth of improper new solutions and discussed in the previous section, causes the collapse of the profiles from 50% to 0% (consistent with the strong packing of the iso-GIM curves of Fig. 2(a)), making the feedback controlled system particularly dangerous when working around these high amplitude values.

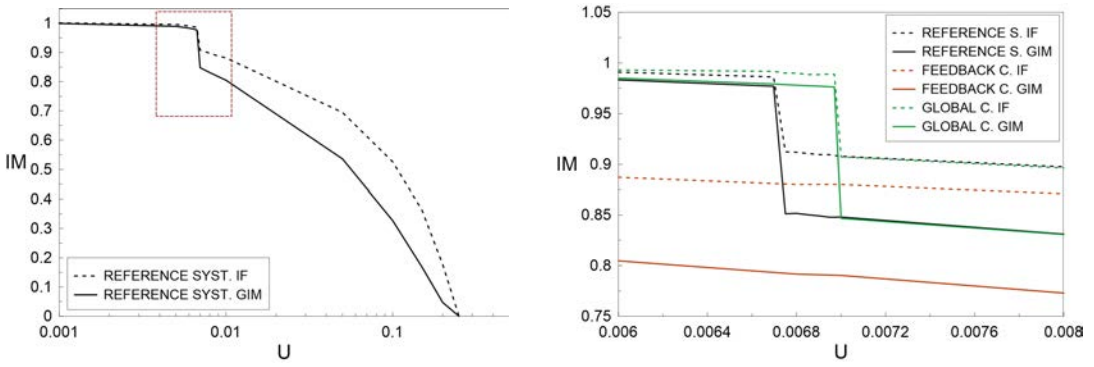

(a) (b)

Fig. 7. Erosion profiles in terms of residual integrity calculated by IF and GIM Integrity Measures (IM) at $\omega = 0.7$ (a) and enlargement (b), as a function of the harmonic forcing amplitude U, with comparison between reference system (black lines), system with feedback control (orange lines) and system with global control (green lines). Continuous lines: GIM; Dashed lines: IF.

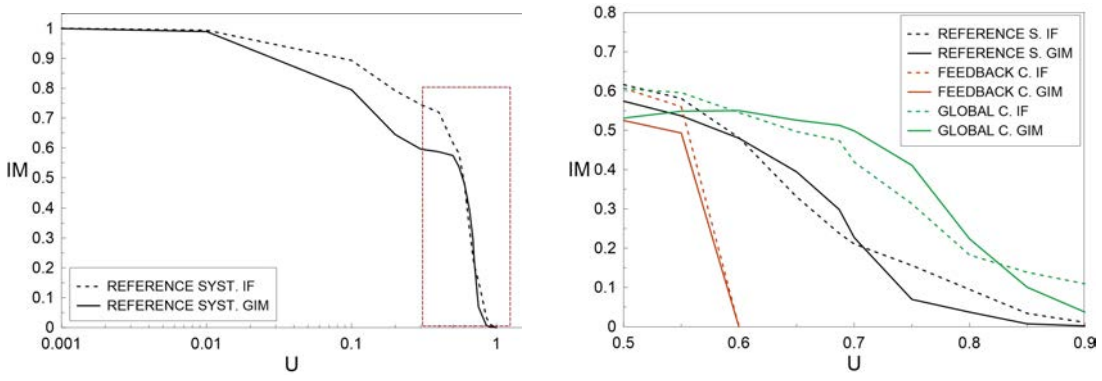

(a) (b)

Fig. 8. Erosion profiles in terms of residual integrity calculated by IF and GIM Integrity Measures (IM) at $\omega = 0.9$ (a) and enlargement (b), as a function of the harmonic forcing amplitude U, with comparison between reference system (black lines), system with feedback control (orange lines) and system with global control (green lines). Continuous lines: GIM; Dashed lines: IF.

Finally, some comments can be drawn comparing the IF (dashed) and GIM (continuous) profiles in Figs. 7 and 8. At the left of the resonance frequency, the erosion develops from the outer edge of the basins, reducing their volume while preserving their compact core. As a consequence, IF is always grater then GIM for all three systems (Fig. 7(b)). At the right of the resonance, the erosion has the aforementioned development for low values of the forcing amplitude (IF > GIM), whereas in the dangerous initial part of the sharper profiles of both the reference and the globally controlled systems the safe basin develops by stretching its overall shape, which maintains the volume almost unchanged while reducing the core (IF < GIM) (Fig. 8(b)).

5. Concluding remarks

Analysis of dynamical integrity has been used as a general framework for evaluating the effects of control techniques to be possibly employed for securing AFM response robustness and safety against jump to contact in different dynamic conditions. Though more systematic investigations could be necessary to reach detailed conclusions, the following main outcomes are in order: (i) External feedback control generally succeeds in satisfactorily keeping the response to a specific suitable one of the reference system in some regions of parameter space, while also producing improper bounded solutions and meaningfully decreasing the overall system safety. (ii) Controls which exploit global properties of the system reference response improve the system safety against jump to contact with variable topological mechanisms, while possibly entailing beneficial effects on the robustness of also specific responses.

References

1. Rega, G., Lenci, S.. A global dynamics perspective for system safety from macro- to nanomechanics: analysis, control and design engineering. *Appl Mech Rev* 2015;**67**(5):050802.
2. Yagasaki, K.. New control methodology of microcantilevers in atomic force microscopy. *Phys Lett A* 2010;**375**:23–28.
3. Lenci, S., Rega, G.. A unified control framework of the nonregular dynamics of mechanical oscillators. *J Sound Vib* 2004;**278**:1051–1080.
4. Hornstein, S., Gottlieb, O.. Nonlinear dynamics, stability and control of the scan process in noncontacting atomic force microscopy. *Nonlinear Dyn* 2008;**54**:93–122.
5. Settimi, V., Gottlieb, O., Rega, G.. Asymptotic analysis of a noncontact AFM microcantilever sensor with external feedback control. *Nonlinear Dyn* 2015;**79**(4):2675–2698.
6. Settimi, V., Rega, G.. Global dynamics and integrity in noncontacting atomic force microscopy with feedback control. *Nonlinear Dyn* 2016; **86**(4):2261–2277.
7. Rega, G., Lenci, S.. Dynamical integrity and control of nonlinear mechanical oscillators. *J Vib Control* 2008;**14**:159–179.
8. Settimi, V., Rega, G.. Exploiting global dynamics of a noncontact atomic force microcantilever to enhance its dynamical robustness via numerical control. *Int J Bif Chaos* 2016;**26**(7):1630018.
9. Rega, G., Settimi, V.. Bifurcation, response scenarios and dynamic integrity in a single-mode model of noncontact atomic force microscopy. *Nonlinear Dyn* 2013;**73**:101–123.